Monthly Notices of the ROYAL ASTRONOMICAL SOCIETY

MNRAS **501,** 4255–4265 (2021) doi:10.1093/mnras/staa3933
Advance Access publication 2020 December 24

Exploring the origin and evolution of the Kepler 36 system

Thomas Rimlinger and Douglas Hamilton
Department of Astronomy, University of Maryland, College Park, MD 20742, USA

Accepted 2020 November 22. Received 2020 November 13; in original form 2019 November 25

ABSTRACT

We examine the origins of the Kepler 36 planetary system, which features two very different planets: Kepler 36b ($\rho = 7.46$ g cm^{-3}) and Kepler 36c ($\rho = 0.89$ g cm^{-3}). The planets lie extremely close to one another, separated by just 0.01 au, and they orbit just a tenth of an au from the host star. In our origin scenario, Kepler 36b starts with far less mass than Kepler 36c, a gaseous giant planet that forms outside the ice line and quickly migrates inwards, capturing its neighbour into its 2:1 mean-motion resonance while continuing to move inwards through a swarm of planetesimals and protoplanets. Subsequent collisions with these smaller bodies knock Kepler 36b out of resonance and raise its mass and density (via self-compression). We find that our scenario can yield planets whose period ratio matches that of Kepler 36b and c, although these successes are rare, occurring in just 1.2 per cent of cases. However, since systems like Kepler 36 are themselves rare, this is not necessarily a drawback.

Key words: planets and satellites: dynamical evolution and stability.

1 INTRODUCTION

1.1 Previous work

Among the most dynamically interesting extra-solar planets (exoplanets) are those in so-called tightly packed systems, which feature multiple bodies all orbiting close both to their host star and to each other. One such system is Kepler 36 (Table 1).

These planets have two notable features. First, they are located very near one another and are also within 1 per cent of the 7:6 orbital mean motion resonance (MMR), i.e. their periods are very close to a 7:6 ratio. Secondly, their densities differ by nearly a factor of 10 despite their small radial separation. The placement of a gaseous sub-Neptune so close to a rocky super-Earth defies standard formation models that predict planetary systems to be segregated by both mass and density, as the Solar system is. This paper proposes a new evolutionary path in which these planets migrate past other more common resonances and terminate at the 7:6 MMR in their current locations.

Several works instead posit that high-energy protostellar radiation might significantly alter these planets' atmospheres (Lopez, Fortney & Miller 2012; Lopez & Fortney 2013; Owen & Morton 2016; Bodenheimer et al. 2018). They argue that the elevated X-ray and XUV (extreme ultraviolet) flux of a young star could strip the atmospheres of high-density, close-in planets. In their now-standard model, Lopez & Fortney (2013) initialize both planets at their current orbits with identical H/He mass fractions (∼22 per cent) and radii ($\sim 10\ R_\oplus$) but different masses ($m_b \sim 5.7\ M_\oplus$, $m_c \sim 9.4\ M_\oplus$) and bulk densities ($\rho_b \sim 0.031$ g cm^{-3}, $\rho_c \sim 0.052$ g cm^{-3}). Kepler 36b loses nearly all of its atmosphere to high-energy stellar radiation within 10^8 yr, while Kepler 36c retains roughly half of its own envelope. The authors attribute this difference to Kepler 36c's greater assumed amount of rocky material (7.34 $M_\oplus$ compared to 4.45 $M_\oplus$ for Kepler 36b) and predict that Kepler 36b should lose its envelope approximately three times faster than Kepler 36c despite receiving only about 24 per cent more radiation. Since they receive similar amounts of radiation, the planets' atmosphere retention rates are largely determined by their core masses; by fine-tuning them, the authors reproduce the observed masses and densities of the Kepler 36 planets. Owen & Morton (2016) and Bodenheimer et al. (2018) study similar formation scenarios without fundamentally modifying the idea that stellar XUV radiation is responsible for the density disparity between these two planets.

More generally, Lopez & Fortney (2013) predict that the incidence of sub-Neptune planets ($1.8 < \text{radius} < 4.0\ R_\oplus$) should decline rapidly for periods $\lesssim$10 d, while the incidence of smaller planets should simultaneously rise. In Fig. 1, we compare these predictions to the modern planetary data base found at exoplanet.eu (Schneider et al. 2011). Current observations show that while the frequency of sub-Neptunes does decline for shorter periods, this decline begins at ∼4 d, much closer than the 10-d prediction of Lopez & Fortney (2013). A steady increase in the number of small planets as the stellar distance decreases from 10 to 1 d periods is also apparent in Fig. 1. The correlation between these two trends is not strong.

Raymond et al. (2018) study a scenario in which the density disparity between the planets is due entirely to the composition of their feeding zones. In their picture, Kepler 36b is rocky because it is formed from the mergers of several rocky bodies totalling 3 $M_\oplus$; likewise for Kepler 36c and two icy bodies totalling 7.3 $M_\oplus$. These are reasonably close to the planets' current observed masses. Stellar radiation is ignored. Once Kepler 36c forms, it migrates inwards towards Kepler 36b, skipping past several resonances but stopping in the 7:6 MMR with Kepler 36b, in which the two planets reside for the remainder of the simulation. While this idea for the density disparity is compelling, we find that convergent migration alone is unlikely to account for the 7:6 MMR. Our simulations (Section 2) indicate that collisions are necessary to eject bodies from resonance, and in their

* E-mail: trimling@umd.edu (TR); dphamil@umd.edu (DH)

Table 1. Key properties of Kepler 36b and c. Data taken from Carter et al. (2012).

Name	Semimajor axis (au)	Density (g cm^{-3})	Mass (M$_\oplus$)
Kepler 36b	0.1153 ± 0.0015	$7.46^{+0.74}_{-0.59}$	$4.45^{+0.33}_{-0.27}$
Kepler 36c	0.1283 ± 0.0016	$0.89^{+0.07}_{-0.05}$	$8.08^{+0.60}_{-0.46}$

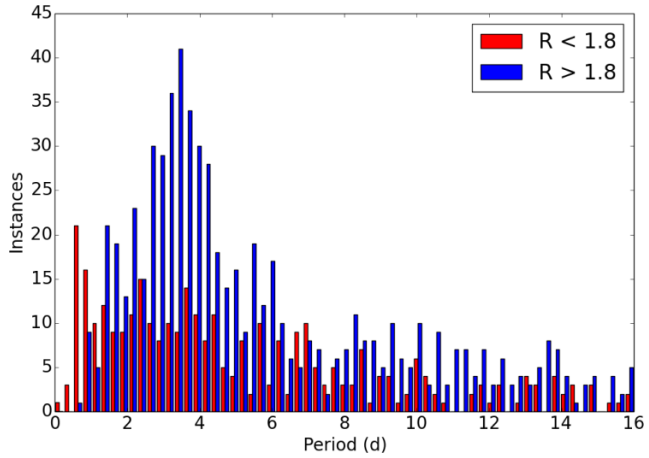

Figure 1. Instances of confirmed planets with period $P < 16$ d, radius $R < 4$ R$_\oplus$, and period and radius errors less than one per cent, using 64 bins. The red bars correspond to planets with $R < 1.8$ R$_\oplus$, which Lopez & Fortney (2013) designate as super-Earths. The blue bars conversely correspond to those planets they designate as sub-Neptunes. Sub-Neptune frequency begins to notably decline at $P \sim 4$ d. Data taken from the exoplanet.eu catalogue (Schneider et al. 2011) and current as of 2020 May 18.

absence, it is difficult to force planets so close together. Furthermore, Quillen, Bodman & Moore (2013) find that stochastically forced planets that capture into the 7:6 resonance from disc forces alone are unlikely to stay there permanently.

Quillen et al. (2013) investigate a different model, in which they place numerous Mars-mass planetary embryos beyond the two planetary orbits; the embryos migrate inwards until they collide with one of the planets, typically the outermost body. After fine tuning the number of embryos, the migration rate, and other parameters, Quillen et al. (2013) find that these collisions can force the planets past several resonances in which they would otherwise remained trapped. In their scenarios, impacts with embryos that stripped one planet (assumed to have already differentiated) of its less dense outer material produced the density contrast. Quillen et al. (2013) suggested two possible formation pathways. In the first, the outer planet (which received approximately twice as many impacts as the inner) lost its mantle, and subsequent collisions kicked it past the inner planet, i.e. the planets exchanged positions. In the second, the inner planet was stripped instead, and no such exchange occurred. Each scenario faces significant difficulties reproducing the density contrast; either the planets had to cross orbits without going unstable, or the planet receiving fewer impacts had to lose its mantle while the planet receiving more could not.

Although this model has many appealing aspects, we do not expect Mars-mass embryos to necessarily migrate inwards faster than planets with an order of magnitude more mass. Quillen et al. (2013) assume that the planets would open gaps in the gas disc (Type II migration), whereas the embryos would not (Type I migration), and that this difference would yield a faster migration rate for the embryos. However, the precise mass range at which planets transition from Type I to Type II migration, and the nature of migration within this range, has enjoyed considerable debate for decades with few firm conclusions beyond general guidelines (e.g. D'Angelo, Kley & Henning 2003; D'Angelo & Lubow 2008; Kley & Nelson 2012). These analyses are typically subject to various simplifying assumptions about the gas disc itself (Tanaka, Takeuchi & Ward 2002). In particular, Kley & Nelson (2012) estimate that Type II migration should not begin until planetary mass $30M_\oplus$ for a typical disc, which would place both Kepler 36 planets firmly in the Type I range. Furthermore, Tanaka et al. (2002) predict that the Type I migration rate should be proportional to mass (their equation 70), implying that planets should migrate faster than embryos. We therefore adopt this requirement.

1.2 Our model

In this paper, we present a formation model for the Kepler 36 planetary system that incorporates many elements of that proposed by Quillen et al. (2013) but is nevertheless distinct in several ways. In our model, Kepler 36b forms within the ice line with less mass than that which Carter et al. (2012) measured, and Kepler 36c forms beyond the ice line with roughly its current mass, perhaps via a similar process to that outlined by Raymond et al. (2018). The two planets migrate inwards through a protoplanetary disc; Kepler 36c migrates faster, rapidly overtaking its less massive neighbour and capturing it into the 2:1 MMR. After this capture, the two planets migrate in together through a field of embryos and small protoplanets. The inner planet is pushed inwards into undepleted parts of the disc and interacts with these bodies, colliding and merging with many of them. Most small planetesimals are gone at this point, having merged to form the larger planetary embryos. Those that remain play no role in the dynamical evolution of the two planets. In this model, most of the embryo/protoplanet disc accretes on to the inner planet, as it migrates inwards. Its mass roughly equals the mass of the accreted material, typically ranging from a few to several Earth masses (see Fig. 8 in Section 3.4).

The likelihood of the smaller bodies colliding with the inner planet, rather than scattering, depends on the inner planet's escape speed $v_{\rm esc}$ and the smaller body's orbital speed $v_{\rm orb}$; they preferentially collide for $v_{\rm esc} < v_{\rm orb}$ and preferentially scatter for $v_{\rm orb} < v_{\rm esc}$ (Goldreich, Lithwick & Sari 2004). Planet b has a radius of 1.486 ± 0.035 R$_\oplus$ (Carter et al. 2012); its mass is given in Table 1. These values yield $v_{\rm esc} \approx 19.4$ km s^{-1}. This allows us to estimate a critical semimajor axis $a_{\rm crit}$ below which an object would preferentially collide with planet b by equating $v_{\rm esc}$ with average orbital velocity $\langle v_{\rm orb} \rangle \approx \sqrt{\frac{GM}{a_{\rm crit}}} \left(1 - \frac{1}{4}e^2\right)$, where G is the gravitational constant, M is the mass of Kepler 36, and a and e are the semimajor axis and eccentricity of the smaller body, respectively. Taking $e = 0.2$, this yields $a_{\rm crit} \approx 2.57$ au, somewhat lower than typical ice line estimates for a Sun-like star (see e.g. Hayashi 1981; Podolak & Zucker 2004; Martin & Livio 2012). Since we model the inner planet as forming within the ice line and migrating inwards, we therefore expect that most close approaches with it should result in collisions, not scattering. As a result, the innermost planet can effectively shield the outermost from the material, as a cowcatcher leading a train shields it from debris on the tracks.

Importantly, some of the collisions are of sufficient strength to eject Kepler 36b from its resonance entirely. Depending on the direction of impact, either the planet is kicked inwards and is quickly recaptured by the inwardly moving 2:1 resonance, or it is flung outwards and is soon captured by a closer resonance, e.g. the 3:2. These outcomes

each occur with a ∼50 per cent probability. We envision that this process repeats until the planets are left near the 7:6 resonance. Additionally, the accretion of denser material not only raises the bulk density of planet b but also increases its mass to the current measured value; the greater self-gravity also acts to further raise the planet's density by compression. Earth has a density of 5.5 g cm^{-3}, a value enhanced by compression of its iron core, and 4.5 $M_\oplus$ of Earth-like material could easily have an average density of 7.5 g cm^{-3}.

2 SIMULATIONS

2.1 Damping forces

To test our model, we used the symplectic option within the *N*-body integrator HNBody (Rauch & Hamilton 2002) to simulate two planets orbiting Kepler 36 in a protoplanetary disc. In addition to the normal gravitational forces between the three bodies in the integration, we also included two additional forces via HNDrag, an expansion suite to HNBody, that approximated the semimajor axis drag ($\dot{a}$) and eccentricity damping ($\dot{e}$) effects of the disc. We modelled $\dot{a}$ with the user-defined force per unit mass $\boldsymbol{f}_a = -k_a$, for planetary velocity and strength $k_a = -\frac{\dot{a}}{2a}$. This force has the useful property that $\dot{e} = 0$ when averaged over an orbit. We define the e damping force by $\boldsymbol{f}_e = -k_e v_r \hat{\boldsymbol{s}}$, where v_r is the radial speed, $\hat{\boldsymbol{s}}$ is a unit vector perpendicular to the overall velocity (minimizing changes to the body's energy), and k_e is analogous to k_a. The velocities in these forces are expressed in units of initial circular velocity of whichever body to which they are applied, approximately equal to 22.3 km s^{-1} for planet b and 14.1 km s^{-1} for planet c. With this normalization, $k_a{}^{-1}$ and $k_e{}^{-1}$ are the approximate time-scales of $\dot{a}$ and $\dot{e}$, respectively.

These forces are clearly simplifications of the true forces these planets would experience in a protoplanetary disc. Quillen et al. (2013) and Malhotra (1993), who investigated the strengths of different orbital resonances in the Solar nebula, suggest two alternatives. Malhotra (1993) considers small planetesimals in a turbulent disc that feel aerodynamic gas drag (Adachi, Hayashi & Nakazawa 1976). She assumes $\boldsymbol{F}_d = -K u \boldsymbol{u}$, where $K \approx \frac{\pi s^2}{4m}$ for radius s and mass m of the body and $\boldsymbol{u} =$ − gas, where and gas are the velocities of the planetesimal and gas, respectively. By contrast, Quillen et al. (2013) use a Stokes drag-like force: $\boldsymbol{F}_d = -\frac{}{2\tau_a} - \frac{-c}{\tau_e}$, where and $_c$ are the planet's velocity and circular velocity at its current radius, respectively, and τ_a and τ_e are the migration and eccentricity damping time-scales, respectively.[1] Malhotra (1993) notes that such a force would be appropriate for a laminar (smooth) disc. Kley & Nelson (2012) also assume a viscous, laminar disc for most of their discussion of migration rates.

2.2 Collisions

We also included collisions, approximated as impulses (changes in velocity δ), in our simulations. This technique offered several advantages over the more traditional approach of directly integrating the impactors along with Kepler 36 and its two planets.

First, we could guarantee that a precise number of impacts would occur, whereas integrating the impactors would have allowed the possibility of no impacts or too many. Clearly, collisions *could* occur in some cases; we simply integrated under the assumption that they did. Secondly, simulating collisions as impulses gave us perfect control over when they occurred, in what direction, and with what strength, enabling us to easily study and understand the effects of a single collision in great detail. Finally, simulating collisions as impulses dramatically reduced integration time and allowed us to simulate arbitrary numbers of collisions at little extra cost. Since integration time is (n^2) for n bodies, directly integrating, e.g. 10 impactors in addition to the star and two planets would have increased our computation time by a factor of nearly 20.

[1] Our drag model is the same as Quillan's when orbit averaged.

Table 2. All parameter values used for the two planets in our simulations: planetary mass (m), semimajor axis (a), eccentricity (e), inclination (i), longitude of ascending node (Ω), longitude of periapse ( ), and true longitude (λ). Quantities separated by commas indicate the different values we used for that parameter. The initial mass of the outer body (8.08 $M_\oplus$) corresponds to its current observed mass, whereas that of the inner body (3.30 $M_\oplus$) is considerably less than today's value. The very small inclinations on each body were imposed to allow inclination resonances, but as they are very weak, our integrations remained close to two-dimensional.

Parameter	Kepler 36b	Kepler 36c
m (M_{star})	10^{-5}	2.42659×10^{-5}
a (au)	2	5
e	0.01	0.01
i (°)	0.002	0.007
Ω, , λ (°)	0	0
k_a ($\times 10^{-7}$ yr^{-1})	0.5, 1, 2	4
$\frac{k_e}{k_a}$	1, 3, 10, 30, 100, 300	1, 3, 10, 30, 100, 300
# Collisions	3, 4, ..., 15	0

We spaced our impacts at intervals of 5 × 10^5 yr; the number of impulses N ranged between 3 and 15 per simulation. For each of our thirteen choices of N, we randomly generated five sets of N values for $\frac{\delta}{v}$ (for 65 sets total); these values were randomly distributed between −0.05 and 0.05 to ensure that most impulses would be able to kick planets out of resonance (see Section 3.2). We selected our range for N by estimating the minimum and maximum number of collisions needed to move the planets from the 2:1 MMR to the 7:6 without going beyond it. We thought it highly unlikely that only one or two collisions could knock the bodies across so many resonances. Even if this were possible, and even assuming they kicked the planets towards each other, such powerful collisions could potentially deviate from our perfect-accretion impulse model quite significantly, e.g. could shatter the impacted body. For our maximum case, we considered the 'unlucky' scenario in which only $\frac{1}{3}$ of the impulses pushed the planets together, and each one moved the planets into the next-closest first-order MMR, for 15 impulses total. Of course, we could have raised this maximum by allowing an even less 'lucky' scenario, but we estimated each of our impactors to be several to tens of lunar masses (Section 3.2). We wished to avoid adding too much rocky mass to a system that already had several times that of the Solar system's terrestrial planets.

Impulses with positive δ were parallel to the impacted planet's velocity, and those with negative δ were antiparallel. For each set of disc parameters (Table 2), we ran five simulations, each using a different set of impulses. All simulations with the same N used the same five impulse strength sets. The timing scheme was not random; we chose a uniform interval that was much longer than the e damping time-scales that we tested. Our tests of different uniform intervals found only minor differences. In any case, it is not obvious what a more 'natural' timing distribution would have looked like. We searched for simulations in which the two planets ended in the 7:6 MMR and separately evaluated how physically likely those scenarios were.

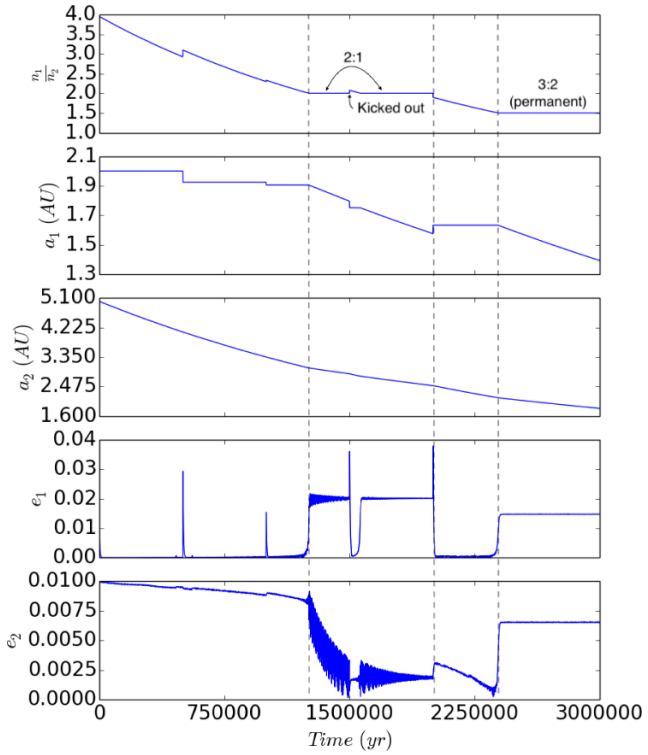

Figure 2. Sample integration. We plot the mean motion ratio $\frac{n_1}{n_2}$, semimajor axes a_1 and a_2, and eccentricities e_1 and e_2 of both planets. The subscripts 1 and 2 denote Kepler 36b and c, respectively. Initial planetary masses and orbital elements are as in Table 2. The inner planet feels no drag force (i.e. $k_{a,1} = 0$), while $k_{a,2} = 4 \times 10^{-7}$ yr^{-1}. The eccentricity damping strengths are $k_{e,1} = 3 \times 10^{-4}$ yr^{-1} and $k_{e,2} = 10^{-7}$ yr^{-1}. The vertical dashed lines mark entrance into ($\sim$1.25 $\times$ 10^6 yr) and exit from (2.0 $\times$ 10^6 yr) the 2:1 MMR as well as entrance into the 3:2 MMR ($\sim$2.4 $\times$ 10^6 yr). The effects of collisions at 0.5, 1.0, 1.5, and 2.0 $\times$ 10^6 yr are readily apparent, particularly in the e_1 plot.

Our impulse approximation for collisions forced us to estimate the impactor masses. Thus, we assigned an orbit with eccentricity e_i to each impactor and assumed perfect angular momentum conservation, i.e. no loss of fragments:

$$m_{\rm i}\boldsymbol{r}_{\rm i} \times \quad_{\rm i} + m_{\rm p}\boldsymbol{r}_{\rm p} \times \quad_{\rm p} = (m_{\rm i} + m_{\rm p})\boldsymbol{r}_{\rm f} \times \quad_{\rm f}, \tag{1}$$

where $\boldsymbol{r}$ and , respectively, denote position and velocity, m denotes mass, and the subscripts i, p, and f , respectively, denote impactor, planet, and final. At time of impact, $\boldsymbol{r}_{\rm i} = \boldsymbol{r}_{\rm p}$ and $_{\rm i} \approx (v_{\rm p} + e_{\rm i} v_{\rm p,circ})\hat{}_{\rm p}$ for planetary circular speed $v_{\rm p,circ}$. With these substitutions, we could solve for $m_{\rm i}$, given two subsequent simulation outputs, where the state vectors from the first output provided $\boldsymbol{r}_{\rm p}$ and $_{\rm p}$, and those from the second provided $\boldsymbol{r}_{\rm f}$ and $_{\rm f}$.

This approach led to some small errors. While in principle, our mass calculation algorithm depended on our output frequency, in practice, we output coordinates frequently enough that each planet's angular momentum changed very little from one output step to the next; changing this frequency introduced differences of order $\lesssim 1$ per cent to the calculated mass, a value far below the uncertainty in the assumed impactor eccentricity. Most significantly, we did not update Kepler 36b's mass within the simulation after each impulse. Since the planet masses are comparable and the inner planet often increased in mass by a third or more, not updating Kepler 36b's mass also introduced some error into our integrations; for example, more massive bodies require more powerful kicks to eject from resonance.

2.3 Initial conditions

We performed over 7000 simulations using the University of Maryland supercomputer deepthought2, in which we varied five parameters: the inner planet's migration rate, inner and outer planet eccentricity damping strengths, number of impulses, and set of impulse strengths. The values that we used for the first four of these parameters as well as planetary masses and initial orbital elements are given in Table 2. All integrations ran for 10^7 yr except for cases in which the inner body got within 0.1 au of the star, at which point our time-step of 0.001 yr was too long to reliably resolve the orbital motion and the simulation came to a pre-programmed halt. Under these conditions, most simulations ended with the two planets near Kepler 36b and c's observed semimajor axes – each sits just over 0.1 au from Kepler 36 (Table 1). In cases featuring powerful collisions that kicked Kepler 36b out past c, however, the planets could end up far apart from each other, as the new, faster-migrating inner planet moved away from the new outer planet until it got within 0.1 au of the star and the simulation ended.

HNBody printed the bodies' state vectors once per thousand years. We prioritized searching a wide parameter space – and finding integrations in which the planets evolved to the current observed Kepler 36 planetary configuration – over confining ourselves to values consistent with a 'standard' protoplanetary disc. We do not know, for example, whether the planets opened a gap in the disc, whether the disc was vertically isothermal, the strength of the disc's viscosity or self-gravity, etc. Furthermore, given that the Kepler 36 system is unusual, the disc in which it evolved may have likewise been unusual. In any case, the specific migration rates of each planet are less important than the relative migration rate of the outer body to the inner one because the relative rate determines how quickly Kepler 36c can 'catch up' to Kepler 36b, which in turn drives the resonance dynamics.

3 RESULTS

3.1 Sample simulation

In general, our individual simulations display diverse resonance and impact phenomena, as we illustrate in a custom sample simulation (Fig. 2). We include migratory and eccentricity damping forces to mimic the effects of nebular gas and arrange for four impacts to occur on the inner planet at intervals of 5 $\times$ 10^5 yr. For simplicity, only the outer planet feels a migratory force. The inner planet's eccentricity damping force is 3000 times stronger than that of the outer planet. These choices allow us to easily see how the planets' semimajor axes and eccentricities respond to resonance capture and departure. As in the rest of our simulations, we follow the planets' evolution for 10^7 yr, although we only show the first 3 $\times$ 10^6 yr in Fig. 2.

At $\sim$1.25 $\times$ 10^6 yr, the planets enter the 2:1 MMR. In the top panel, this is immediately evident from the constant mean-motion ratio. Resonance capture is likewise responsible for the changed migration rates in the next two panels; as the inner planet starts moving inwards, the outer planet slows somewhat. Finally, the establishment of non-zero eccentricity equilibria in the bottom two panels also tracks resonance capture. At 1.5 $\times$ 10^6 yr, the inner planet collides with another embryo and is kicked radially inwards, out of the 2:1 MMR; Kepler 36b's migration ceases and the e_1 equilibrium is destroyed.

Due to its faster migration rate, the outer body eventually recaptures the inner body into the 2:1 MMR, and they move in as a unit until 2 $\times$ 10^6 yr, whereupon the inner body is hit with yet another